CHEMISTRY OF MATERIALS

Article

pubs.acs.org/cm

# Kinetics of Anatase Electrodes: The Role of Ordering, Anisotropy, and Shape Memory Effects

Anna A. Belak, Yizhou Wang,† and Anton Van der Ven*

Department of Materials Science and Engineering, University of Michigan, Ann Arbor, Michigan, 48109, USA

Supporting Information

**ABSTRACT:** We perform a comprehensive first-principles statistical mechanical study of the thermodynamic and kinetic properties of lithiated anatase $Li_xTiO_2$. We establish that the experimentally observed step in the voltage vs lithium composition curve between $x = 0.5$ and 0.6 is due to Li ordering. Furthermore, we predict that full lithiation of anatase $TiO_2$ is thermodynamically possible at positive voltages but that there is an enormous difference in Li diffusion coefficients in the dilute and fully lithiated forms of $TiO_2$, providing an explanation for the limited capacity in large electrode particles. We also predict that Li diffusion in the ordered phase ($Li_{0.5}TiO_2$) is strictly one-dimensional. The $TiO_2$ to $Li_{0.5}TiO_2$ phase transition has much in common with shape memory alloys. Crystallographically, it can support strain invariant interfaces separating $TiO_2$ and $Li_{0.5}TiO_2$ within the same particle. The strain invariant interfaces are parallel to the one-dimensional diffusion direction in $Li_{0.5}TiO_2$, which, we argue, has important consequences for the role of particle shape on achievable capacity, charge and discharge rates, and hysteresis.

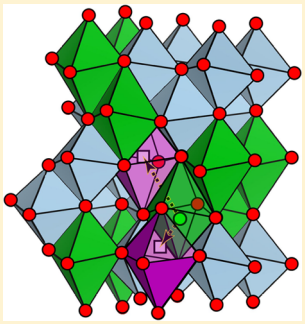

**KEYWORDS:** *lithium ion battery, anatase, $TiO_2$, electrode material, shape memory, diffusion*

## INTRODUCTION

Lithium battery materials are remarkable in their ability to undergo large variations in Li concentration at room temperature. This phenomenon requires large open spaces, a low susceptibility to dramatic phase transitions, and high ion mobilities. Anatase $TiO_2$ has been extensively studied over the past decade due to its potential applications in photovoltaic,[1,2] electrochromic,[2] and electrochemical[1,3−8] devices, showing promise as a viable electrode material for Li batteries.

Anatase has a tetragonal unit cell that can theoretically accommodate one lithium for every titanium. Upon lithiation to $Li_{0.5}TiO_2$, anatase is observed to undergo a tetragonal to orthorhombic phase transition. This composition is also most frequently reported as the maximum electrochemical insertion limit of Li into bulk anatase, although concentrations as high as 0.6 have been reported.[4,9,10] Only with nanostructured anatase $TiO_2$ has the theoretical capacity of $x = 1.0$ been reached.[11] It has been suggested that the limited capacity of bulk anatase is due to a low Li diffusion coefficient in the fully lithiated phase.[11,12] Here we report on a first-principles study of the thermodynamic and kinetic properties of lithiated anatase $TiO_2$ and provide crucial insight about the role of kinetic and crystallographic properties of anatase $TiO_2$ in limiting the achievable capacity to slightly more than half of its theoretical value. We find that the thermodynamically stable ordered phase at $x = 0.5$ can accommodate excess Li over vacant sites up to $x = 0.6$ and that Li diffusion in this phase is strictly one-dimensional at room temperature with a diffusion coefficient that is lower than that of Li diffusion in anatase $TiO_2$. We also predict that the Li diffusion coefficient in the fully lithiated phase, $LiTiO_2$, is several orders of magnitude lower than that in $TiO_2$ and $Li_{0.5}TiO_2$ due to the absence of distorted Ti−O octahedra that opens up the Li diffusion path in dilute $TiO_2$. We argue that this is responsible for capping the achievable capacity of anatase $TiO_2$ to approximately half of its theoretical value in bulk crystallites.

Our analysis also points to a strong coupling between kinetic behavior and electrode particle shape, providing new insights as to how morphology can be exploited to enhance charge and discharge rates and minimize hysteresis. The dimensional changes accompanying the tetragonal $TiO_2$ to orthorhombic $Li_{0.5}TiO_2$ transition satisfy conditions for a strain invariant interface separating the two phases when they coexist in the same particle. The transformation therefore should have much in common with those occurring in shape memory alloys. The predicted one-dimensional diffusion direction in $Li_{0.5}TiO_2$, however, is parallel to the strain invariant interface and has no component toward those interfaces. This suggests that large, coarse particle morphologies that are susceptible to a core-shell two-phase mechanism will lead to limited capacity and rates.

## RESULTS AND DISCUSSION

We performed a comprehensive study of phase stability using the cluster expansion formalism[13] as implemented in the CASM code.[14] As a first step, we enumerated a large number of Li-vacancy configurations over the octahedral sites of anatase $TiO_2$, calculating the energies of 188 of them with Density Functional Theory (DFT) using the VASP code (Supporting

**Received:** March 20, 2012
**Revised:** June 22, 2012
**Published:** June 26, 2012

   dx.doi.org/10.1021/cm300881t | *Chem. Mater.* 2012, 24, 2894−2898

Information).[15−17] The calculated formation energies confirm the stability of the ordered phase at $x = 0.5$, predicted by Morgan and Watson[18] with similarities to that proposed by Wagemaker et al.[19] This phase is responsible for the step in the voltage vs lithium composition curve. The ordered phase is characterized by a zigzag arrangement of Li and vacancies causing an expansion along the $b$ axis and a contraction along the $c$ axis of the anatase host with little change in the $a$ lattice parameter. These dimensional changes break the tetragonal symmetry of the anatase host, reducing it to an orthorhombic space group. The predicted lattice parameters of the ordering at $x = 0.5$ are $a = 3.81$ Å, $b = 8.21$ Å, and $c = 9.20$ Å (anatase: $a = b = 3.81$ Å, $c = 9.68$ Å), which are in good agreement with experimental neutron diffraction measurements by Cava et al.[20,21] The unique lithium-vacancy ordering of this structure results in a larger primitive unit cell (doubling of the original $a$ axis of anatase along the $b$ direction) and places it in the *Pnnm* (No. 58) space group, as illustrated in Figure 1. The structure's

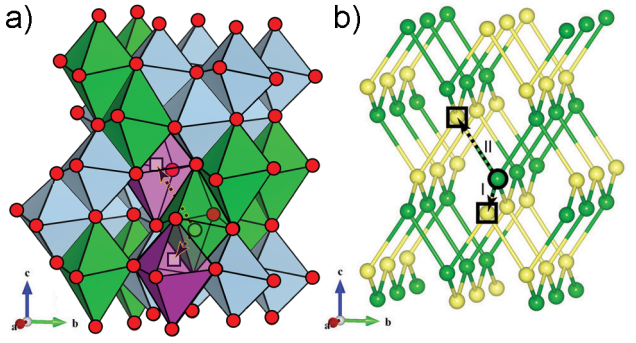


**Figure 1.** Lithium-vacancy ordering of the $\beta$-$Li_{0.5}TiO_2$ phase. In (a), the lithium, titanium, and vacancy octahedra are green, blue, and purple, respectively. In (b), only the lithium (green) and vacancy (yellow) sublattices are shown. The arrows indicate possible diffusion hop paths.

Wyckoff positions are reported in Table S1 (Supporting Information). We will refer to this ordered phase as $\beta$, using $\alpha$ to denote anatase $TiO_2$, potentially having a dilute Li concentration, and $\gamma$ to denote fully lithiated anatase, $LiTiO_2$.

The first-principles formation energies of the 188 Li-vacancy configurations were used to construct cluster expansions for the configurational energy: one for the dilute limit and a second to describe the energy of $\beta$-$Li_xTiO_2$ as a function of configurational excitations relative to its perfectly ordered state at $x = 0.5$. The cluster expansions were implemented in Monte Carlo simulations to calculate free energies and chemical potentials as a function of Li concentration. The voltage is related to minus the Li chemical potential according to the Nernst equation. Figure 2 shows the predicted voltage vs lithium composition curve at room temperature (300 K). It is characterized by two large plateaus separated by a step around $x = 0.5$. The step between $x = 0.5$ and 0.58 emerges from the stability of $\beta$-$Li_xTiO_2$. Monte Carlo simulations reveal that ordered $\beta$-$Li_{0.5}TiO_2$ can easily accommodate additional Li over its vacant sites up to a composition of $x = 0.58$. In contrast, the removal of Li from the Li sublattice in $\beta$-$Li_{0.5}TiO_2$ results in a large energy penalty, thereby limiting the stability of $\beta$-$Li_xTiO_2$ between 0.5 and 0.58. The first plateau arises from a two-phase coexistence between $\alpha$-$Li_{0.1}TiO_2$ and $\beta$-$Li_{0.5}TiO_2$, and the second plateau is due to a two-phase coexistence between $\beta$-$Li_{0.58}TiO_2$ and $\gamma$-$Li_{1.0}TiO_2$. The prediction that the second

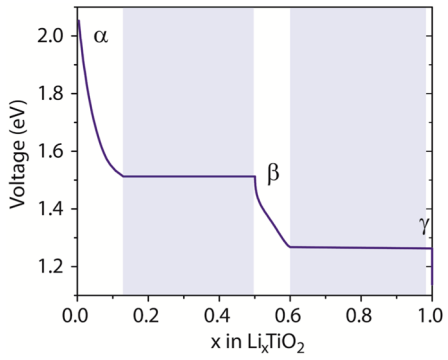


**Figure 2.** The calculated voltage vs lithium composition curve for $Li_xTiO_2$ at 300 K was obtained using grand canonical Monte Carlo simulations with a cluster expansion. The blue shading indicates two phase regions.

plateau is well above zero volts indicates that the limit in achievable capacity is not thermodynamic in origin but rather kinetic. For most insertion compounds, voltage vs lithium composition curves predicted with methods relying on approximations to DFT are systematically underpredicted. For example, the first plateau is predicted to occur at 1.5 V, while experimentally it is measured around 1.78 V.[6]

In order to elucidate the behavior of anatase during charge and discharge, we investigated the mechanisms with which Li ions diffuse within the $\alpha$, $\beta$, and $\gamma$ forms of anatase $Li_xTiO_2$. We used the nudged elastic band (NEB) method as implemented in VASP to calculate the activation barriers for a variety of possible diffusion hops in $\alpha$-, $\beta$-, and $\gamma$-$Li_xTiO_2$ and kinetic Monte Carlo simulations to calculate macroscopic diffusion coefficients as described elsewhere.[14,22]

In $\alpha$-$Li_xTiO_2$, where the Li concentration is dilute, all of the available sites are equivalent, and all hops into adjacent vacancies are symmetrically identical. Lithium ions occupying octahedral sites within transition metal oxide and sulfide insertion compounds typically perform curved hops, passing through an adjacent tetrahedral site.[14,23] In anatase, however, the adjacent tetrahedral sites between neighboring Li octahedra share faces with two Ti containing octahedra. The strong electrostatic repulsion from these face-sharing Ti renders the tetrahedral sites unstable, forcing Li to pass through more constricted octahedron edges, whereby it has to squeeze between two edge-forming oxygen atoms, as illustrated in Figure 3. The octahedral sites that can accommodate lithium in

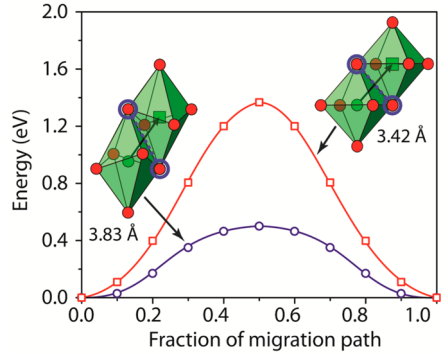


**Figure 3.** The minimal energy migration paths in the dilute $\alpha$ phase (blue circles) and fully lithiated $\gamma$ phase (red squares) are calculated with the nudged elastic band method in VASP.


dx.doi.org/10.1021/cm300881t | *Chem. Mater.* 2012, 24, 2894−2898

anatase $TiO_2$ are noticeably distorted due to the presence of $Ti^{4+}$ with edge lengths (O−O interatomic distance) varying between 3.08 Å and 3.77 Å. In the fully lithiated $\gamma$-$LiTiO_2$, in contrast, the octahedral distortions are absent due to the change in the effective Ti valence from 4+ to 3+ upon addition of Li to anatase $TiO_2$. The edge lengths of the octahedra are now uniform and noticeably smaller at 2.96 Å. This change in edge length with Li concentration has important consequences for the Li migration barriers. Calculated migration barriers in dilute anatase and in fully lithiated anatase (containing one vacancy) are shown in Figure 3, from which it is clear that as the octahedral distortions disappear with Li concentration, creating more uniform edges, it becomes more difficult for a diffusing atom to pass between the two oxygen atoms that form the octahedron edge. This results in the much higher barrier of 1.37 eV for a hop in $\gamma$-$LiTiO_2$ than a corresponding 0.50 eV barrier in dilute $\alpha$-$Li_xTiO_2$, in which the octahedral distortions separate the pair of oxygen ions adjacent to the activated state. This large difference in migration barrier leads to an astounding almost 15 orders of magnitude drop in the chemical diffusion coefficient when going from dilute anatase to fully lithiated anatase.

Each Li within the zigzag ordering of $\beta$-$Li_xTiO_2$ is coordinated by one other lithium atom and three vacant sites, two of which are symmetrically equivalent. As a consequence, two symmetrically distinct hops of lithium atoms into adjacent vacant sites are now allowed, as shown in Figure 1. An atom hopping along path II travels 3.68 Å in the $a-c$ plane while an atom hopping along path I only travels 2.46 Å in the $b-c$ plane. These large differences in hop distances are correlated with large differences in migration barriers, with an activation barrier of 1.55 eV along the long path II, which is much higher than the barrier along the short path I of only 0.78 eV, as shown in Figure 4. Similar trends were found for Li hops within $\beta$-$Li_xTiO_2$ after the introduction of local disorder due, for example, to slight deviations from stoichiometry. Such a dramatic difference in activation barriers for the two hop paths suggests the possibility of one-dimensional diffusion along the $a$ axis in $\beta$-$Li_xTiO_2$.

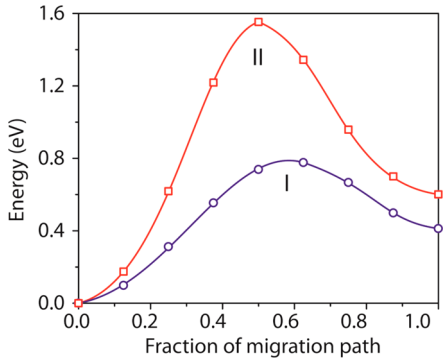


**Figure 4.** Minimal energy migration path for the two symmetrically distinct hops available to a diffusing lithium atom in $\beta$-$Li_{0.5}TiO_2$. The barrier for hop I (blue circles) is much smaller than the barrier for hop II (red squares).

We used our cluster expansion in combination with kinetic Monte Carlo (KMC) simulations as implemented in the CASM code to calculate the diffusion coefficients for lithium atoms in $Li_xTiO_2$ at different lithium compositions. The diffusion coefficient, $D$, appearing in Fick's first law can be written as a product of a thermodynamic factor, $\Theta$, and a kinetic factor, $D_J$, referred to as a self- or intrinsic diffusion coefficient.[24] The thermodynamic factor measures the deviation from thermodynamic ideality and is related to the derivative of the Li chemical potential with respect to the natural log of the Li concentration. The self-diffusion coefficient can be calculated with KMC by evaluating a Kubo-Green expression.[24] A more detailed explanation of these concepts and methods is available elsewhere.[25]

Figure 5 shows the chemical diffusion coefficient as a function of Li concentration. The diffusion coefficient is slightly anisotropic in $\alpha$ and $\gamma$ (the difference is not discernible on the logarithmic scale of Figure 5). In the $\beta$ phase, extensive KMC simulations at 300 K showed that 100% of the hops occurred along path I, implying that hops along path II are negligible at room temperature and diffusion in the ordered $\beta$ phase is one-dimensional (along the $a$ axis). At low concentration, $D$ is comparable to that of other insertion compounds. Our predicted value of $2 \times 10^{-11}$ $cm^2/s$ is likely an upper bound as we neglect interactions between Li and localized electronic states, which tend to reduce Li mobility especially at dilute concentrations.[26] $D$ drops substantially at $x = 0.5$ to about $10^{-16}$ $cm^2/s$. In the fully lithiated phase, $LiTiO_2$, the absence of distorted Ti−O octahedra results in an even larger drop in the chemical diffusion coefficient to a value of $6 \times 10^{-26}$ $cm^2/s$.

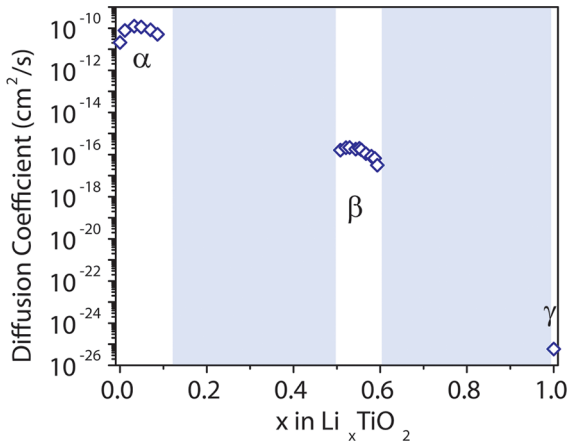


**Figure 5.** Chemical (blue diamonds) diffusion coefficient in the $a$ direction is plotted as a function of lithium concentration at 300 K. The blue shading indicates two phase regions.

Our thermodynamic and kinetic predictions provide crucial insight to rationalize and overcome the cycling and capacity limitations of anatase. One key prediction is the very low Li diffusion coefficient in the fully lithiated phase, which explains the limited capacity of anatase electrodes. Our thermodynamic predictions indicate that fully lithiated $\gamma$-$LiTiO_2$ should form through a two-phase reaction from $\beta$-$Li_{0.58}TiO_2$. One mechanism for such a reaction is with a core-shell morphology where the new, Li-rich, $\gamma$-$LiTiO_2$ phase forms on the surface of the electrode particles and grows inward consuming the $\beta$-$Li_{0.58}TiO_2$ as Li is supplied to the particle. In order for Li to reach the two-phase reaction front, however, it must diffuse through $\gamma$-$LiTiO_2$, which has enveloped the surface. The exceedingly low Li diffusion coefficient in $\gamma$-$LiTiO_2$ will prevent any substantial ingress of Li once a thin layer of $\gamma$-$LiTiO_2$ covers the particle surface. This effectively limits the maximum Li concentration of anatase to the solubility limit of $\beta$-$Li_{0.5}TiO_2$,


dx.doi.org/10.1021/cm300881t | Chem. Mater. 2012, 24, 2894−2898

which our thermodynamic analysis indicates is about 0.6, in excellent agreement with practically achievable capacities in anatase.[4,9,10] Only for the smallest nanoparticles of anatase can we expect higher Li concentrations, when diffusion distances are so small that diffusion is no longer rate-limiting.[27,28] In this context, Borghols et al. were able to show that smaller nanoparticles of anatase can be lithiated more successfully than larger ones. In fact, 7 nm nanoparticles can be fully lithiated to $x = 1.0$.[11] Similarly, Bresser et al. have reported capacities up to $x = 0.75$ for 3−4 nm diameter anatase nanorods.[29]

Our results also shed light on the $\alpha$-$TiO_2$ to $\beta$-$Li_{0.5}TiO_2$ two-phase reaction, which has been studied extensively experimentally.[10,20,21] While the $a$-axis of anatase ($\alpha$-$TiO_2$) and of $\beta$-$Li_{0.5}TiO_2$ have negligible misfit (0.1%), the $c$-axis contracts by 5.0%, and the $b$-axis expands by 7.7% when transforming from $\alpha$-$TiO_2$ to $\beta$-$Li_{0.5}TiO_2$. Within a two-phase reaction model, characterized by a transient two-phase coexistence within each individual particle, such a large lattice misfit typically results in significant coherency strain energies.[30] Unique to this particular two-phase reaction, however, is that the misfit strains are restricted to the $b$−$c$ plane of $\beta$-$Li_{0.5}TiO_2$, with contraction along $c$ and expansion along $b$. As is well-known from the study of martensitic transformations in metallurgy, this condition results in planes that are common to both $\alpha$-$TiO_2$ and $\beta$-$Li_{0.5}TiO_2$ with zero misfit strain.[31] Two-phase morphologies within single particles are therefore possible without introducing coherency strains, provided that the interface between $\alpha$ and $\beta$ is parallel to any of the strain invariant planes. For the tetragonal to orthorhombic transformation between $\alpha$ and $\beta$, the strain free interfaces will be parallel to the (0, 0.207, ±0.064) and (0.207, 0, ±0.064) habit planes in the anatase crystal coordinate system.[31]

Since the strain invariant planes in $\beta$ are perpendicular to the $b$−$c$ plane and, therefore, parallel to the $a$-axis (the direction of Li diffusion in $\beta$), Li diffusion in $\beta$ can only occur parallel to the reaction front and not toward the reaction front. Hence, diffusion through newly formed $\beta$ is unlikely to contribute to its further growth. Instead, Li must be supplied from the $\alpha$-$TiO_2$ side of the reaction front, as illustrated in Figure 6a. This is only possible if the $\alpha$ phase extends to the surface of the particle throughout the two-phase reaction to allow additional Li to enter the crystal. Any particle shapes that promote a core-shell growth mechanism, with $\beta$ covering the whole particle, as shown in Figure 6b, are undesirable as they would rapidly cut off the Li supply to the moving interface. To ensure full completion of the two-phase reaction, the moving interface must extend to the surface of the particle (Figure 6a) such that a fresh $\alpha$-$TiO_2$ surface is always exposed to enable additional Li to enter the crystal. This is more likely in plate-like particles that are thin in the [001] direction.

For large anatase particles, several variants of $\beta$-$Li_{0.5}TiO_2$ could nucleate on different parts of the surface. As these nuclei, having different orientations relative to the original anatase particle, grow inward, they will start impinging, resulting in an increase in elastic strain energy. Overcoming the elastic strain energy for continued growth requires an under potential during discharge, thereby resulting in hysteresis in the voltage vs lithium composition curve. Stresses arising from the coexistence of several orthorhombic variants within the original anatase particle could also become large enough to cause particle fracture, leading to electrode degradation.

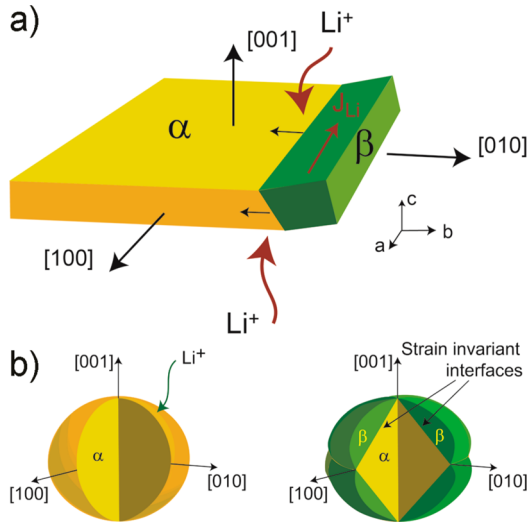


**Figure 6.** The strain-invariant interface between $\alpha$ and $\beta$ is parallel to the one-dimensional lithium diffusion direction in $\beta$. A two-phase reaction will require Li addition through the original $\alpha$ phase, which is more likely in plate-like particles (a) than in large coarse particles (b) that are more susceptible to a core-shell mechanism.

## CONCLUSIONS

We have calculated key thermodynamic and kinetic properties of lithiated anatase from first principles, allowing us to shed light on the origins of important limitations of this insertion compound in Li-ion battery applications. Our prediction of a remarkably low Li diffusion coefficient in $LiTiO_2$ and a high solubility limit of ordered $Li_{0.5}TiO_2$ explains the limited capacity of $x = 0.6$. The $TiO_2$ to $Li_{0.5}TiO_2$ transformation has much in common with martensitic phase transformations, exhibiting strain invariant planes for two-phase coexistence. Furthermore, we predict one-dimensional Li diffusion within ordered $Li_{0.5}TiO_2$ in a direction parallel to the strain invariant planes between anatase $TiO_2$ and ordered $Li_{0.5}TiO_2$, implying that Li must enter electrode particles at $TiO_2$ exposed surfaces. This insight provides clear guidance as to how capacity and rates can be maximized and hysteresis minimized during the $\alpha$ to $\beta$ transformation by controlling particle shape relative to crystallographic directions of anatase.

## ASSOCIATED CONTENT

### Supporting Information

Computational details, CIF, and Wyckoff table for $\beta$-$Li_{0.5}TiO_2$, and VASP total energy and lattice parameter plots. This material is available free of charge via the Internet at http://pubs.acs.org.

## AUTHOR INFORMATION

### Corresponding Author

*E-mail: avdv@umich.edu.

### Present Address

†Department of Mechanical Engineering, University of California, Berkeley, CA.

### Notes

The authors declare no competing financial interest.

## ACKNOWLEDGMENTS

This material is based upon work supported as part of the Northeastern Center for Chemical Energy Storage, an Energy

Frontier Research Center funded by the U.S. Department of Energy, Office of Science, Office of Basic Energy Sciences under Award No. DESC0001294. Computational resources provided by TERAGRID DMR100093 are also gratefully acknowledged. Images of crystal structures were produced with VESTA.[32]

## REFERENCES

(1) Kavan, L.; Grätzel, M.; Gilbert, S. E.; Klemenz, C.; Scheel, H. J. *J. Am. Chem. Soc.* **1996**, *118*, 6716.
(2) Grätzel, M. *Inorg. Chem.* **2005**, *44*, 6841.
(3) Ohzuku, T.; Hirai, T. *Electrochim. Acta* **1982**, *27*, 1263.
(4) Bonino, F.; Busani, L.; Lazzari, M.; Manstretta, M.; Rivolta, B.; Scrosati, B. *J. Power Sources* **1981**, *6*, 261.
(5) Ohzuku, T.; Takehara, Z.; Yoshizawa, S. *Electrochim. Acta* **1979**, *24*, 219.
(6) Ohzuku, T.; Kodama, T.; Hirai, T. *J. Power Sources* **1985**, *14*, 153.
(7) Macklin, W. J.; Neat, R. J. *Solid State Ionics* **1992**, *53*−*56*, 694.
(8) Huang, S. Y.; Kavan, L.; Exnar, I.; Gratzel, M. *J. Electrochem. Soc.* **1995**, *142*, L142.
(9) Whittingham, M. S.; Dines, M. B. *J. Electrochem. Soc.* **1977**, *124*, 1387.
(10) Zachau-Christiansen, B.; West, K.; Jacobsen, T.; Atlung, S. *Solid State Ionics* **1988**, *28*−*30*, 1176.
(11) Borghols, W. J. H.; Lützenkirchen-Hecht, D.; Haake, U.; van Eck, E. R. H.; Mulder, F. M.; Wagemaker, M. *Phys. Chem. Chem. Phys.* **2009**, *11*, 5742.
(12) Wagemaker, M.; Kearley, G. J.; van Well, A. A.; Mutka, H.; Mulder, F. M. *J. Am. Chem. Soc.* **2003**, *125*, 840−848.
(13) Sanchez, J. M.; Ducastelle, F.; Gratias, D. *Physica A* **1984**, *128*, 334.
(14) Van der Ven, A.; Thomas, J. C.; Xu, Q.; Swoboda, B.; Morgan, D. *Phys. Rev. B* **2008**, *78*, 104306.
(15) Kresse, G.; Furthmüller, J. *Phys. Rev. B* **1996**, *54*, 11169.
(16) Blochl, P. E. *Phys. Rev. B* **1994**, *50*, 17953.
(17) Kresse, G.; Joubert, D. *Phys. Rev. B* **1999**, *59*, 1758.
(18) Morgan, B. J.; Watson, G. W. *J. Phys. Chem. Lett.* **2011**, *2*, 1657.
(19) Wagemaker, M.; Borghols, W. J. H.; Mulder, F. M. *J. Am. Chem. Soc.* **2007**, *129*, 4323.
(20) Murphy, D. W.; Cava, R. J.; Zahurak, S. M.; Santoro, A. *Solid State Ionics* **1983**, *9&10*, 413.
(21) Cava, R. J.; Murphy, D. W.; Zahurak, S.; Santoro, A.; Roth, R. S. *J. Solid State Chem.* **1984**, *53*, 64.
(22) Bhattacharya, J.; Van der Ven, A. *Phys. Rev. B* **2010**, *81*, 104304.
(23) Bhattacharya, J.; Van der Ven, A. *Phys. Rev. B* **2011**, *83*, 144302.
(24) Gomer, R. *Rep. Prog. Phys.* **1990**, *53*, 917.
(25) Van der Ven, A.; Bhattacharya, J.; Belak, A. A. *Acc. Chem. Res.* **2012**, DOI: 10.1021/ar200329r.
(26) Morgan, B. J.; Watson, G. W. *Phys. Rev. B* **2010**, *82*, 144119.
(27) Sudant, G.; Baudrin, E.; Larcher, D.; Tarascon, J.-M. *J. Mater. Chem.* **2005**, *15*, 1263.
(28) Shin, J.-Y.; Samuelis, D.; Maier, J. *Adv. Funct. Mater.* **2011**, *21*, 3464.
(29) Bresser, D.; Paillard, E.; Binetti, E.; Krueger, S.; Striccoli, M.; Winter, M.; Passerini, S. *J. Power Sources* **2012**, *206*, 301−309.
(30) Van der Ven, A.; Garikipati, K.; Kim, S.; Wagemaker, M. *J. Electrochem. Soc.* **2009**, *156*, A949.
(31) Christian, J. W. *Metall. Mater. Trans. A.* **1994**, *25*, 1821.
(32) Momma, K.; Izumi, F. *J. Appl. Crystallogr.* **2008**, *41*, 653.